Journal of
Composites Science

MDPI

Article

New Perspectives on Zirconia Composites as Biomaterials

Giuseppe Magnani, Paride Fabbri, Enrico Leoni, Elena Salernitano and Francesca Mazzanti *

ENEA, Laboratory of Materials Technologies Faenza, Via Ravegnana 186, 48018 Faenza, Italy; giuseppe.magnani@enea.it (G.M.); paride.fabbri@enea.it (P.F.); enrico.leoni@enea.it (E.L.); elena.salernitano@enea.it (E.S.)
* Correspondence: francesca.mazzanti@enea.it

Abstract: Zirconia–alumina composites couple the high toughness of zirconia with the peculiar properties of alumina, i.e., hardness, wear, and chemical resistance, so they are considered promising materials for orthopedic and dental implants. The design of high performance zirconia composites needs to consider different aspects, such as the type and amount of stabilizer and the sintering process, that affect the mechanics of toughening and, hence, the mechanical properties. In this study, several stabilizers (Y_2O_3, CuO, Ta_2O_5, and CeO_2) were tested together with different sintering processes to analyze the in situ toughening mechanism induced by the tetragonal–monoclinic (t–m) transformation of zirconia. One of the most important outcomes is the comprehension of the opposite effect played by the grain size and the tetragonality of the zirconia lattice on mechanical properties, such as fracture toughness and bending strength. These results allow for the design of materials with customized properties and open new perspectives for the development of high-performance zirconia composites for orthopedic implants with high hydrothermal resistance. Moreover, a near-net shape forming process based on the additive manufacturing technology of digital light processing (DLP) was also studied to produce ceramic dental implants with a new type of resin–ceramic powder mixture. This represents a new frontier in the development of zirconia composites thanks to the possibility to obtain a customized component with limited consumption of material and reduced machining costs.

Keywords: zirconia–alumina composite; stabilizing oxides; critical grain size; tetragonality; mechanical properties; fracture toughness; flexural strength; ceramic additive manufacturing; DLP

Citation: Magnani, G.; Fabbri, P.; Leoni, E.; Salernitano, E.; Mazzanti, F. New Perspectives on Zirconia Composites as Biomaterials. *J. Compos. Sci.* **2021**, *5*, 244. https://doi.org/10.3390/jcs5090244

Academic Editor: Francesco Tornabene

Received: 30 July 2021
Accepted: 7 September 2021
Published: 11 September 2021

1. Introduction

Zirconia-toughened alumina (ZTA) and alumina-toughened zirconia (ATZ) composites have been studied for many decades to overcome some drawbacks of the tetragonal zirconia polycrystal (TZP) [1–3]. Zirconia–alumina composites have been used for several years as load-bearing biomaterials [4–6]. They combine the high toughness and strength of zirconia with the high hardness and stiffness of alumina, and they show also an increased hydrothermal stability of the tetragonal zirconia phase. It is well-known that the stress-induced tetragonal-to-monoclinic (t–m) transformation of zirconia results in fracture toughness improvement [7–11] due to energy-dissipative mechanisms and the inhibition of crack tip propagation [12]. Characteristics such as grain size, the type and amount of stabilizer, and the sintering process strongly affect the tetragonal zirconia transformability and the transformation toughening mechanism. In fact, the grain size of tetragonal zirconia has to be maintained below a critical size to reach a high value of fracture toughness [13].

Many oxides have already been tested as stabilizers to increase the metastability of the tetragonal phase by means of varying the c/a ratio of the elementary cell. The c/a ratio of the tetragonal phase is generally known as "tetragonality" and is an indicator of the distortion of the t-ZrO_2 unit-cell, hence the instability. On the other hand, alumina addition increases matrix stiffness and exerts a constraint on zirconia particles, maintaining them in the metastable tetragonal state [14,15] and acting as a "mechanical stabilizer".

One of the main problems of zirconia-based compounds as biomaterials is the sensitivity of 3Y-TZP (3 mol% yttria tetragonal zirconia polycrystal) ceramics to low temperature degradation (LTD) when they are in contact with water that is already at human body temperature or water vapor [16]. The inherent presence of oxygen vacancies, generated when Y^{3+} replaces Zr^{4+} in the cationic sub-lattice, can be at the origin of aging, since they can be refilled by hydroxyl groups in the presence of water [17]. As a result of the LTD process, the t–m transformation of zirconia grains spontaneously occurs without any external applied stress. The correlated volume expansion results in the formation of microcracks that can catastrophically damage orthopedic or dental prostheses. In the literature, many data regarding the lifetime estimation of Y-TZP and ATZ or ZTA composites have been collected [18–22]. Accelerated aging tests in steam and hot water at low temperatures (e.g., 90–134 °C) are the accepted methods to simulate an in vivo aging behavior with the determination of activation energy value for environmentally driven t–m transformation. Fabbri et al. [21] studied a ZTA composite that showed a very low reactivity to the LTD compared to 3Y-TZP. This behavior of ZTA composites confirms that the presence of alumina grains can act as a barrier for the propagation of phase transformation to the neighboring zirconia grains, promoting the higher hydrothermal stability of the tetragonal phase [23–25]. Other studies have evaluated the possibility to significantly retard the hydrothermal degradation of Y-TZPs with small amounts of alumina addition. This result is attributed to the segregated Al^{3+} at the grain boundary of zirconia [24,26–28] without compromising the mechanical properties [17,29,30]. LTD is also influenced by the microstructure. Halmann et al. [31] showed that a finer microstructure had a beneficial effect on the LTD of Y-TZP. At the same time, a finer microstructure does not always affect the mechanical properties, such as flexural strength and fracture toughness, of zirconia-based materials in a positive manner [12,32–36]. In any case, all the previous studies confirmed that alumina–zirconia composites represent an improvement in terms of LTD resistance.

In last two decades, additive manufacturing (AM) technology has been brought from research or niche and expensive industrial applications to everyone thanks to the cost reduction of 3D printers. AM has been demonstrated to be effective in almost every material field and in multiple applications. The digital light processing (DLP) technique consists of the light-induced, layer-by-layer polymerization of a photocurable resin filled with ceramic powders. This technique allows for the manufacturing of relative dense ceramic components, with high degree of detail and surface finishing, that can be advantageously applied in, for instance, the biomedical field (bone scaffolds), the sector of metal-free dental restoration (endosseous implants and dental crowns), and microelectronics (sensors). 3D printing can be considered to be the most promising near net-shape forming technique for technical ceramics. In fact, it has opened the space for application in sectors where high manufacturing costs, connected to the machining costs (30–50% to the total manufacturing costs), usually prevent ceramic use [37]. In addition to the economical evaluation, we should also consider the important aspects related to the realization of parts with completely new designs and positive impacts on environmental sustainability due to the limited production of wastes and the sustainable use of raw materials. Finally, zirconia-based composites represent a new class of materials for applications with 3D printing technologies [38–42]: the need for the complex or customized shapes required in the field of biomaterials could be more easily satisfied by AM techniques. Additional studies are, however, required in order to demonstrate that AM can be conveniently applied to zirconia–alumina composites to produce reliable components.

In this paper, a comprehensive study of the effects of different parameters, i.e., type and amount of stabilizers, sintering thermal cycles, on the mechanical properties of zirconia-based materials, is described along with a demonstration of the applicability of the DLP AM technique for the manufacturing of zirconia–alumina-based dental elements.

2. Materials and Methods

2.1. Ceramic Mixtures and Sample Preparation

Yttria-stabilized zirconia (TZ-3YB, Tosoh, Tokyo, Japan), monoclinic zirconia (TZ0, Tosoh, Tokyo, Japan), alumina (Baikalox SM8, Baikowski Chimie, Poisy, France), chromium (III) oxide, tantalum (V) oxide, copper (II) oxide, and cerium (IV) oxide (99.9%, Carlo Erba, Milano, Italy) powders were mixed in the weight ratios reported in Table 1. The average particle was is 40 nm for both zirconia powders, 120 nm for alumina, and 0.7–1 µm for the other powders (Ta_2O_5, CeO_2, CuO, and Cr_2O_3).

Table 1. List of zirconia and zirconia composites considered in the present study.

Samples	ZrO_2-3Y (wt%)	ZrO_2-TZ0 (wt%)	Ta_2O_5 (wt%)	CeO_2 (wt%)	CuO (wt%)	Al_2O_3 (wt%)	Cr_2O_3 (wt%)
Zr3Y	100	-	-	-	-	-	-
Zr2Y	67.2	32.8	-	-	-	-	-
Zr3YTa	99.85	-	0.15	-	-	-	-
ZrCe	-	84	-	16	-	-	-
Zr3YCu	99.9	-	-	-	0.1	-	-
20803Y	80	-	-	-	-	20	-
50502Y	33.42	16.32	-	-	-	50	-
50502.5Y	41.8	8.2	-	-	-	50	-
50503Y	50	-	-	-	-	50	-
60402Y	26.8	13.08	-	-	-	59.52	0.60
60403Y	39.88	-	-	-	-	59.52	0.60

In case of ZTA or zirconia stabilized with oxides, a slurry (38.5 wt% of solid) was prepared using water as a solvent and 1 wt% of dolapix PC33 (Zschimmer & Schwarz, Lahnstein, Germany) as a dispersant; this slurry was homogenized with a Turbula mixer for 8 h in the presence of 3 mm zirconia spheres.

The slurry was dried with an IR lamp or by freeze-drying. The freeze-drying process was performed with an apparatus composed by a vacuum chamber paired with a vacuum pump through a cold trap filled with liquid nitrogen. The slurry (25 wt% of solid) was granulated in a liquid nitrogen bath with an ultrasonic nebulizer probe. The frozen granules were placed in the chamber under an active vacuum. The temperature of the frozen slurry was naturally maintained at about −20 °C by the heat removed during the water sublimation. The freeze-drying process ended when the powder naturally reached room temperature and the pressure decreased to 0.1 Pa.

The green samples were prepared by die pressing at 60–80 MPa, followed by cold isostatic pressing (CIP) at 100–150 MPa.

2.2. Ceramic Resin and 3D Printing

The ATZ resin was prepared by mixing liquid acrylate monomers (Sartomer, IGM Resins and Allnex), a 405 nm photo-initiator (IGM Resins, Waalwijk, The Netherlands), a commercial zirconia (TZ-3YS, Tosoh, Tokyo, Japan) with an average grain size of 90 nm, and the abovementioned commercial alumina powders with a weight ratio of 80/20. A dispersant (2 wt%) was added to the preparation before the high energy ball milling process to reduce the viscosity of the photocurable ceramic slurries [43]. A solid content in the range of 36–38 vol% of ceramic powder was reached in the slurries in order to obtain a viscosity lower than 1 Pa.s at 10 s^{-1} [44]. A DLP 3D printer (3DLPrinter-HD 2.0+, Robotfactory, Italy; construction volume of L 100 × W 56 × H 150 mm^3) was used and equipped with a projector using a UV–visible high pressure Hg lamp (250 W of power and 3000 lm of luminous flux). The layer height and exposure time for each layer were set in the ranges of 30–50 µm and 6–20 s, respectively. After printing and washing, a post-curing step with a UV lamp was also applied.

2.3. Sintering Process: Thermal Cycles

The green samples were debinded and pressureless solid state sintered (SSS) in flowing air (LINN Elektronik HT—1800 VAC, LINN HIGH THERM GMBH, Hirschbach, Germany). Samples were dewaxed with a cycle up to 800 °C (10 °C/h ramp) in flowing air and then pressureless sintered in flowing air in the range of 1450–1570 °C for different holding times (2–80 h) depending on the composition. The dewaxing and sintering steps for the 3D-printed green bodies were performed at 1550 °C for ATZ for 1 h after a debinding step performed at 800 °C.

In addition, the two-step sintering (TSS) process was also tested. In this case, T_1 and T_2 were in the ranges of 1400–1500 and 1350–1450 °C, respectively, with zirconia and ATZ.

2.4. Physical, Microstructural and Mechanical Characterization

Sintered density was determined by Archimedes' method.

Diffraction patterns were collected by using a Philips X-ray powder diffractometer with Bragg–Brentano geometry and Cu Kα radiation (40 kV and 35 mA) to identify the crystalline phases in the sintered samples and to evaluate the tetragonality of the tetragonal phase.

Viscosity measurements were performed using a Malvern Kinexus Pro+ rheometer (Kinexus pro+, Malvern Instruments, Ltd., Worcestershire, UK) at 25 °C with cone-plate geometry (4°, 40 mm) in shear rate control from 0.1 to 300 s^{-1}.

The microstructural analysis of both the surface and cross sections of sintered bodies was performed with a scanning electron microscope (SEM, LEO 438 VP).

The flexural strength was determined at room temperature with four-point bending tests (five tests for each composition). Samples, in the form of 2 × 2.5 × 25 mm bars, were prepared and tested in accordance with the standard ENV843-1:2004 (cross head speed of 0.5 mm/min and support span of 20 mm). Hardness (H_v) was determined by means of Vickers indentation with a load of 9.8 N, while fracture toughness (K_{IC}) was determined by means of Vickers indentation with a load ranging from 9.8 to 98 N. To calculate fracture toughness, the formula proposed by Niihara [45] for Palmqvist cracks was used (Equation (1)):

$$K_{IC} = \frac{0.035\left(H_v a^{0.5}\right)\left(3\frac{E}{H_v}\right)^{0.4}\left(\frac{l}{a}\right)^{-0.5}}{3} \text{ for } 0.25 < \frac{l}{a} < 2.5 \quad (1)$$

where a is the indent half-diagonal, E is the Young's modulus, and l is the Palmqvist crack length.

3. Results and Discussion

3.1. Stabilization of Zirconia: Variables That Influence Transformability

3.1.1. Type of Stabilizer

Different zirconia-based materials were produced and characterized to study the effect of the type of the stabilizer on the t–m phase transformation. The dopants could be classified according to their oxidation state (Cu^{2+}, Y^{+3}, Ce^{4+}, and Ta^{5+}). More precisely, they are stabilizers of the tetragonal phase (Y_2O_3 and CeO_2) and toughening oxides (Ta_2O_5 and CuO) [46].

Cations' valence and size affect the stabilization mechanism of the tetragonal phase [47–50], even if the correlation is not univocal, as suggested by Yoshimura et al. [51].

The phase composition and crystallographic parameters were evaluated for each mixture (lattice constants c and a and their c/a ratio, namely "tetragonality") of doped tetragonal zirconia. The values of fracture toughness and hardness were also determined (Table 2).

Table 2. Properties of zirconia-based materials doped with different stabilizers and toughening oxides. DR is the relative density, c/a is the tetragonality, K_{IC} the fracture toughness, and H_V the microhardness.

Samples	DR (%)	Tetragonal ph. (vol%)	Monoclinic ph. (vol%)	c/a	K_{IC} (MPa $m^{1/2}$)	H_V (GPa)
ZrCe	98	100	-	1.0191	18.4 ± 0.9	8.7 ± 0.2
Zr2Y	98	83	17	1.0166	9.4 ± 0.4	12.5 ± 0.5
Zr3Y	99	100	-	1.0159	4.0 ± 0.1	11.0 ± 0.3
Zr3YTa	99	100	-	1.0173	9.4 ± 0.5	12.7 ± 0.4
Zr3YCu	98	100	-	1.0161	4.6 ± 0.2	12.5 ± 0.4

Yttrium oxide (Y_2O_3) is the most common stabilizer of the tetragonal phase, and Y-TZP is widely used due to its strong mechanical properties [26,52]. The addition of different amounts of yttria influenced the c/a ratio, which indicated the transformability of the available tetragonal phase. In comparing the values in Table 2 for the mixtures of Zr2Y and Zr3Y, it is clear that a higher yttria content (3 vs. 2 mol%) led to a greater stabilization of the tetragonal phase, which corresponded to a decrease in the c/a ratio (1.0159 vs. 1.0166) and a lower toughness (4.0 vs. 9.4 MPa $m^{1/2}$).

Cerium oxide (CeO_2) is another well-known stabilizer of zirconia, and ceria-doped zirconia exhibits very high values of fracture toughness [53]. The ZrCe sample in our study showed toughness value four times higher than that of Zr3Y (18.4 vs. 4.0 MPa $m^{1/2}$, respectively) as indicated in Table 2. CeO_2 is a stabilizer as Y_2O_3, but its c/a ratio is higher; this means that the tetragonal phase is less stabilized, so its transformation is easier, thus leading to an increase in fracture toughness. On the other hand, as described in the literature [54], CeO_2 does not allow one to obtain high values of mechanical resistance due to its limited capability to contain grain growth during sintering. Indeed, ZrCe grains are wider (ca. 2.0 μm) than Y-TZP ones (ca. 0.5–0.8 μm) [27]. As the oxidation state is the same of Zr^{4+}, Ce^{4+} does not generate oxygen vacancies inside the ZrO_2 cell, so, in a humid environment, the t–m spontaneous transformation is not promoted and CeO_2-stabilized zirconia shows significantly high resistance to LTD [17,54,55].

Tantalum oxide (Ta_2O_5) is known in the literature for its toughening effect when added to 3Y-TZP [56,57]. In our study, the addition of Ta_2O_5 led to a higher value of fracture toughness than 3Y-TZP (9.4 vs. 4.0 MPa $m^{1/2}$, respectively), as shown in Table 2. The addition of Ta_2O_5 to 3Y-TZP increased the c/a ratio (1.0173 vs. 1.0159, respectively) such that the chemical driving force for the t–m transformation was enhanced, and this led to a higher value of fracture toughness. On the other hand, the stabilizing effect of Y_2O_3 was contrasted by the addition of Ta_2O_5, which is a toughening oxide that increases the t–m martensitic transformation temperature [50], resulting in a toughening effect.

Copper oxide (CuO) was also tested as toughening agent for Y-TZP. The results reported in Table 2 show that the addition of CuO only led to a slight increase in the fracture toughness of the 3Y-TZP (4.6 vs. 4.0 MPa $m^{1/2}$, respectively). This result is in contrast with the results reported by Ramesh et al. [58], where a different Y-TZP powder was used.

After comparing the fracture toughness values (Table 2) as function of the tetragonality, a linear correlation was obtained, as shown in Figure 1. If the c/a ratio of the tetragonal phase was near 1 (i.e., the c/a value of the cubic phase), the tetragonal phase was more stable and hence the t–m transformation became more difficult and the fracture toughness decreased. On the contrary, if the c/a ratio of the tetragonal phase increased up to 1.022 (which is the b/a value of the monoclinic phase), the t–m transformation was favored and the fracture toughness increased.

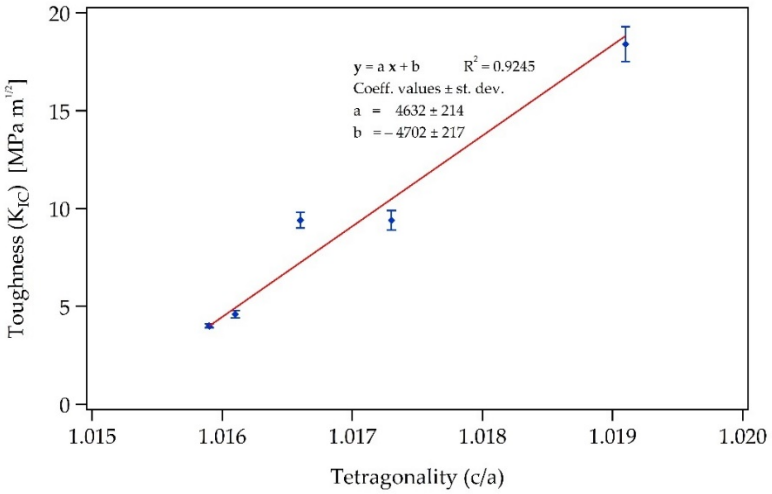

Figure 1. Fracture toughness vs. tetragonality of the different stabilizers in zirconia-based materials.

3.1.2. Stabilizer Content

The effect of different contents of stabilizer (Y_2O_3) was studied in ZTA composites with a 60/40 alumina/zirconia weight ratio. The results reported in Table 3 show that the fracture toughness reached a maximum value of 6.2 MPam$^{1/2}$ with the lowest amount of stabilizer (60402Y). The same results were previously observed in ZTA composites with a 50/50 alumina/zirconia weight ratio, as reported in Table 3 [59].

Table 3. Properties of ZTA materials doped with different amounts of stabilizer. DR is the relative density, c/a is the tetragonality, K_{IC} the fracture toughness, H_V the microhardness, and MOR is the four-point flexural strength.

Samples	DR (%)	c/a	Tetragonal ph. (vol%)	Cubic ph. (vol%)	Monoclinic ph. (vol%)	K_{IC} (MPa m$^{1/2}$)	H_V (GPa)	MOR (MPa)
60403Y	99.9	1.0168	76.3	23.7	0	5.1 ± 0.3	17.7 ± 0.3	660 ± 23
60402Y	98.8	1.0169	98.0	0	2	6.2 ± 0.2	18.0 ± 0.3	794 ± 98
50503Y [1]	99.3	1.0165	98.7	1.3	0	6.0 ± 0.1	14.9 ± 0.5	-
50502.5Y [1]	99.9	1.0170	94.6	5.4	0	5.6 ± 0.2	15.7 ± 0.3	-
50502Y [1]	99.2	1.0175	100	0	0	8.1 ± 0.1	15.4 ± 0.2	-

[1] Reprinted with permission from ref. [59]. Copyright © 2021 Elsevier Ltd.

This behavior can be explained by the analysis of the variation of the tetragonal phase amount and the tetragonality with stabilizer content. In fact, 60403Y had a lower amount of tetragonal phase (less than 80%) and a lower tetragonality than those of 60402Y. This means that a lower quantity of tetragonal phase was available to the toughening t–m transformation in the 60403Y composite. Furthermore, in the same sample, the lower tetragonality enhanced the stability of the tetragonal phase, which caused a decrease in the fracture toughness. These observations are also in line with the study of Yoshimura et al. [60], which reported the dependence of the c/a ratio on stabilizer content.

3.1.3. Critical Grain Size

3Y-TZP was sintered in six different conditions in order to highlight the effect of the grain size variation on tetragonality and, consequently, fracture toughness. The experimental results are reported in the Table 4.

After increasing the sintering time to 60 h at 1550 °C, the fracture toughness and grain size increased up to maximum values of 7.7 MPa m$^{1/2}$ and 1.19 µm, respectively (Figure 2). Furthermore, a strong dependence between the fracture toughness and tetragonality was observed at the microstructural level. Indeed, with the increase in sintering time, tetragonality increased, i.e., the tetragonal cell instability grew. This instability, caused by the distortion of the cell, promoted the t–m transformation and a consequent increase in fracture toughness.

Table 4. Properties of zirconia-based (3Y-TZP) samples sintered with different thermal cycles. DR is the relative density, Dm the average grain size, c/a is the tetragonality, K_{IC} the fracture toughness, and H_V the microhardness.

Thermal Cycle	DR (%)	Dm (μm)	c/a	K_{IC} (MPa $m^{1/2}$)	H_V (GPa)
1500 °C—2 h	98.9	0.53	1.0159	5.0 ± 0.1	11.0 ± 0.2
1550 °C—20 h	99.9	0.78	1.0164	5.3 ± 0.1	12.1 ± 0.2
1550 °C—30 h	99.6	0.87	1.0165	5.4 ± 0.1	11.5 ± 0.2
1550 °C—40 h	99.9	0.95	1.0165	6.6 ± 0.2	11.9 ± 0.2
1550 °C—60 h	99.6	1.19	1.0167	7.7 ± 0.1	11.0 ± 0.2
1550 °C—80 h	95.8	-	1.0162	-	-

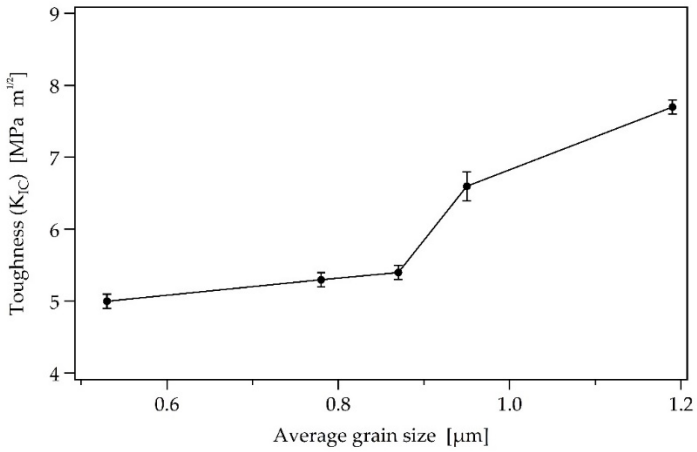

Figure 2. Fracture toughness vs. average grain size of the different sintered zirconia-based materials.

The sample sintered at 1550 °C for 80 h was characterized by the lowest sintered density due to the formation of the monoclinic phase, and it showed many cracks. In fact, XRD analysis confirmed that all the samples were mainly constituted by the tetragonal phase with traces of the cubic phase, while the sample sintered at 80 h showed an increase in monoclinic phase content.

According to these data, the critical grain size can be estimated to be equal or greater than 1.19 μm for this 3Y-TZP material. This value is in agreement with the critical grain observed by Lange [32].

3.2. Parameters That Influence Mechanical Properties

The relationships between the microstructure and mechanical properties of Y-TZP ceramics have been extensively studied over the past four decades, and different effects have been identified.

It was demonstrated that the toughening effect, related to the t–m transformation mechanism in Y-TZP ceramics, is promoted by larger grain sizes [12,32–36]. On the other hand, some mechanical properties, including flexural strength, are known to be enhanced by fine microstructures [36,61,62].

Indeed, as grain size coarsens, the critical defect enlarges, thus leading to a strength decrease [63]. According to the Griffith (Equation (2)), strength (σ_R), fracture toughness (K_{IC}), and failure origin size (c) are strictly connected and their control is necessary to obtain reliable structural ceramic materials.

$$\sigma_R \sim \frac{K_{IC}}{\sqrt{\pi c}} \quad (2)$$

Unfortunately, the best conditions (composition, grain size, transformability, etc.) to reach ceramic strength in zirconia-based materials are not the same for maximizing

fracture toughness, so the reliability of these ceramics comes from the compromise of these two properties [64].

Hardness is also influenced by microstructure [65]. Generally, hardness is strictly related to density, but no univocal correlation between hardness and grain size has been proven. The hardness values of 3Y-TZP do not show the influence of the grain dimension in the submicrometric range [66].

A typical method to obtain ceramics with fine microstructures and improved mechanical properties (flexural strength) is based on the application of innovative sintering processes that limit grain growth. Among the best known sintering methods to refine ceramic microstructures, the spark plasma sintering (SPS) [67,68] and microwave sintering (MWS) [69] methods are the most efficient.

A simple and cost-effective method for industrial applications to obtain near full dense ceramics with controlled grain growth is TSS (two-step sintering) [70], in which the sample is first heated to a higher temperature to achieve an intermediate density and then cooled down and held at a lower temperature until it is fully dense. This sintering method has been successfully applied for ZTA composites [71,72].

The effect of TSS on the 3Y-TZP and ZTA samples (Table 5) was studied and compared to that of classic SSS. In the case of 3Y-TZP, TSS showed an advantageous effect on grain size (almost halved), as shown in Figure 3a,b. However, TSS seemed to have no effect on the fracture toughness. This was probably due to two opposite and concomitant effects of TSS that compensate for each other. The grain size refinement contrasted with the toughening effect achieved when the grain size approached the critical value. On the other hand, the tetragonal phase obtained with the TSS was more transformable, as evidenced by the slight increase in the tetragonality. It is probable that the longer holding time at the higher temperature promoted the migration of the stabilizer (Y^{3+}) [52]; hence, the yttria concentration within the tetragonal phase decreased and enhanced transformability.

Table 5. Properties of 3Y-TZP and ZTA materials sintered with the single step (SSS) or two-step cycles (TSS). DR is the relative density, K_{IC} the fracture toughness, H_V the microhardness, MOR is the four-point flexural strength, Dm is the average grain size (A refers to alumina and Z to zirconia grains), and c/a is the tetragonality.

Samples	Thermal Cycle	DR (%)	Dm A/Z (μm)	c/a	K_{IC} (MPa $m^{1/2}$)	H_V (GPa)	MOR (MPa)
3Y-TZP SSS	1500 °C—1 h	99.7	0.33	1.0154	5.0 ± 0.1	13.3 ± 0.3	1095 ± 75
3Y-TZP TSS	1400/1350 °C—30 h	99.8	0.18	1.0157	4.9 ± 0.1	13.4 ± 0.2	1102 ± 85
60402Y SSS	1550 °C—1 h	98.8	0.71/0.44	1.0169	6.2 ± 0.2	18.0 ± 0.3	794 ± 98
60402Y TSS	1500/1450 °C—30 h	98.6	0.58/0.35	-	5.5 ± 0.3	16.1 ± 0.4	660 ± 89
60402Y TSS FD	1500/1450 °C—30 h	98.7	0.59/0.34	-	-	-	872 ± 47
60403Y SSS	1550 °C—1 h	99.9	0.70/0.43	1.0168	5.1 ± 0.3	17.7 ± 0.3	660 ± 23
60403Y TSS	1500/1450 °C—30 h	99.8	0.58/0.36	-	4.8 ± 0.2	16.0 ± 0.2	700 ± 57

Again, the flexural strength values were very similar despite the halved grain size. It is probable that the grain refinement obtained with TSS did not contribute to a decrease in critical defect size. In fact, as observed by Xiong et al. [73], the TSS method could yield the formation of thermodynamically stable large pores, thus showing its limit in eliminating last residual porosity (1–2%). The effects of grain size refinement and critical defect dimension compensate for each other, thus leaving the strength value unaltered (as also described by Trunec [62]).

In the case of the ZTA composites, the TSS method effectively limited grain growth (Figure 3c,d). Comparing two samples with the same stabilizer content, the grain size refinement resulted in a lower toughness, probably due to the average grain dimension being too far from the critical grain size. The strength values of the 60403Y samples were found to be similar, likely because the increase in the critical defect size was not sufficiently compensated for by the refinement of the microstructure, as suggested by Trunec [62]. For the 60402Y samples, dynamic pore coalescence occurred in the second step of TSS, which did not aid the elimination of residual porosity and had detrimental effects on bending strength [73].

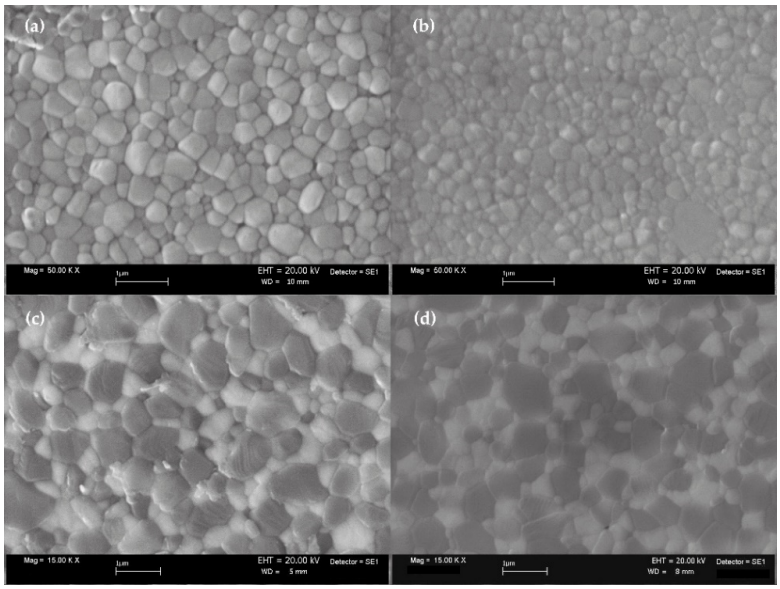

Figure 3. SEM micrographs of zirconia samples 3Y-TZP SSS (**a**) and 3Y-TZP TSS (**b**), as well as of ZTA samples 60403Y SSS (**c**) and 60403Y TSS (**d**).

Finally, the bending strength was also influenced by the powder preparation technique. Using the freeze-drying technique to dry the slurry, the production of a homogeneous granulate without aggregates was achieved (Figure 4). This granulation process strongly influences the quality of a green and sintered body [74]; in our study, higher values of bending strength were obtained (872 ± 47 MPa for 60402Y TSS-FD; see Table 5).

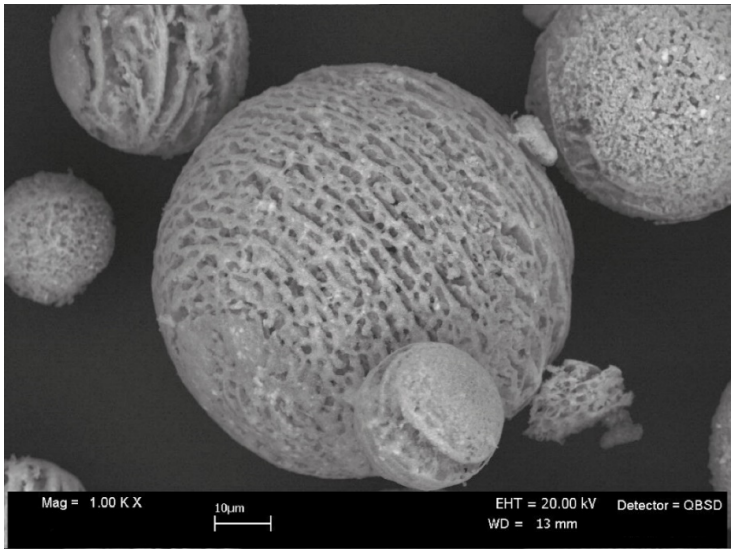

Figure 4. SEM micrograph of 60402Y powder prepared with freeze-dry granulation.

3.3. New Manufacturing Techniques: 3D Printing

The production of ceramic components via the DLP technique is strictly connected to the availability of a suitable ceramic slurry. Nowadays, the most important producers of vat polymerization printers commercialize feedstocks for their 3D printer models with limited possibility to access to other resins available on the market. Another problem for the AM of ceramics with the DLP technique is the low disposability of printable slurries filled with desired ceramic powders.

For the preparation of new resin–ceramic powder mixtures, one of the main problems related to the addition of a high content of ceramic powder to the photopolymeric resin

is the increase in the viscosity of the mixture. This drawback was solved here by wisely selecting monomers with different functionalities and molecular weights. The shear thickening behavior that is commonly observed in high solid loaded suspensions was reduced by the use of an appropriate surfactant and a zirconia powder with a lower surface area (7 ± 2 m^2/g). In this way, high content ceramic photocurable resins (see Materials and Methods section) with low viscosity, suitable for the DLP printing process, were prepared.

The shear viscosity for two ATZ resins is reported in Figure 5.

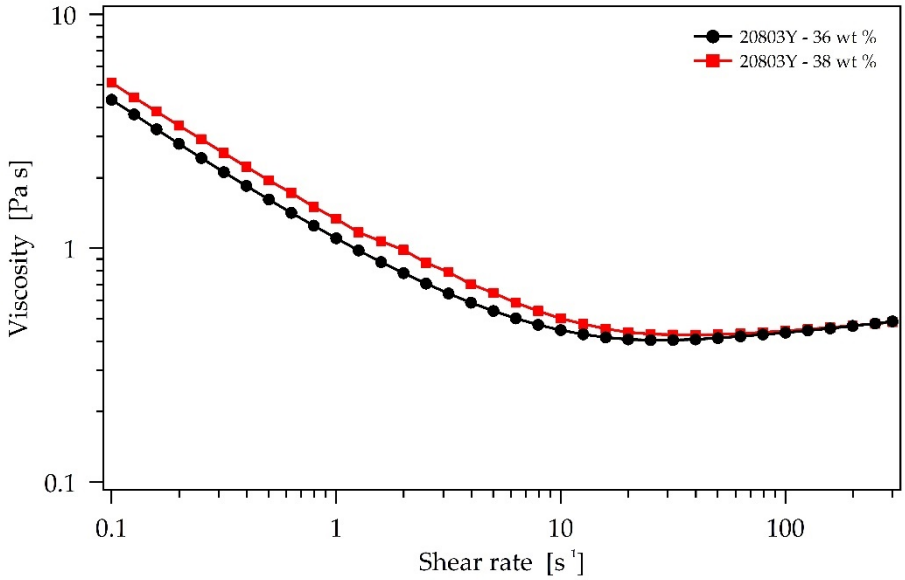

Figure 5. Photocurable slurry viscosity.

Prototypal dental endosseous implants were obtained via the DLP technique with the developed ZTA resin (Figure 6), which was sintered up to 1550 °C for 1 h and reached a final density of 96.8%.

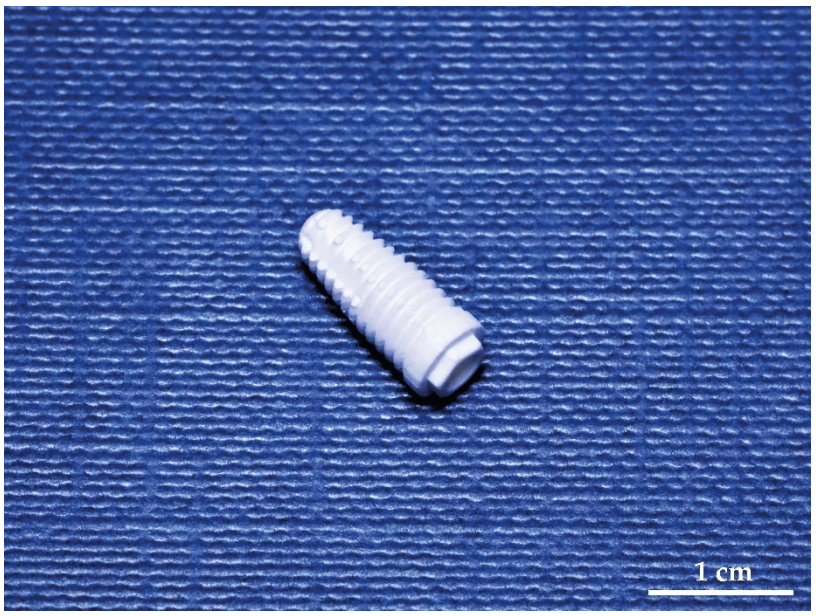

Figure 6. Endosseous dental implant in ATZ printed with the DLP technique.

More complex shapes, as the lattice structure shown in Figure 7, were successfully printed with a final relative density of 98%. Layer-by-layer deposition is highlighted

in Figure 8. SEM observations revealed a regular lattice structure profile, where the overlapping layers and their homogeneity in thickness were clearly visible. The slicing value was set to 50 µm and fell to 35 µm after sintering shrinkage. Nevertheless, the layer adhesion could be further enhanced to completely avoid the delamination defects partially present in these items.

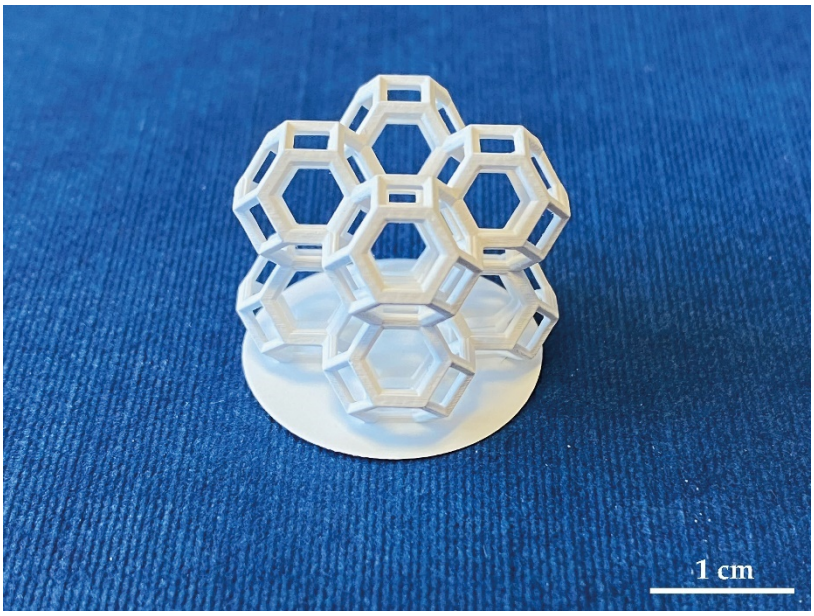

Figure 7. Lattice structure in ATZ printed by the DLP technique.

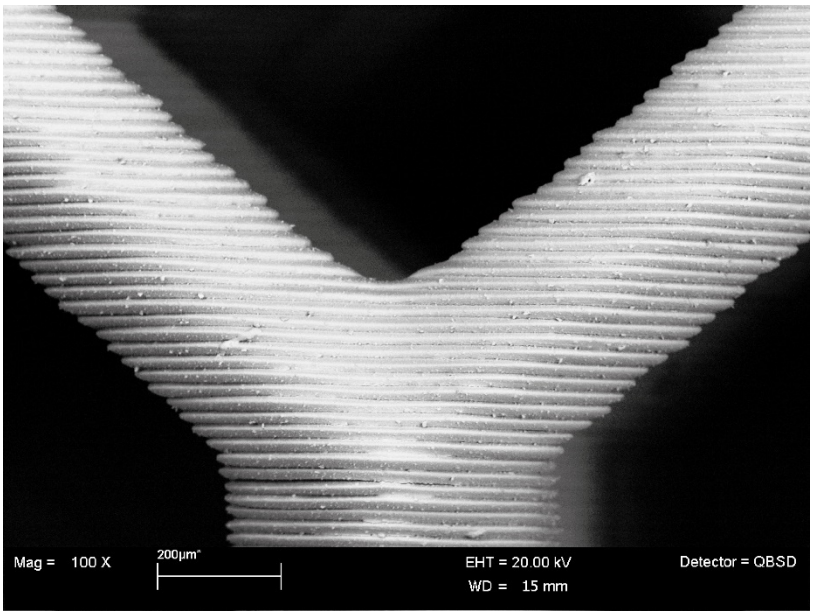

Figure 8. Micrograph of the lattice structure profile.

These preliminary outcomes highlighted the possibility to develop resins with the required ceramic material and the feasibility to print ceramic materials with low cost and widely available DLP printers.

4. Conclusions

Alumina–zirconia composites emphasize the unique properties of zirconia and show many positive aspects that encourage their applications as biomaterials.

The type of stabilizer of the tetragonal phase and the use of toughening oxides with different oxidation states were found to strongly influence the value of the tetragonality, which is the c/a ratio of the lattice parameters of the tetragonal cell. The existence of a linear correlation between tetragonality and fracture toughness was verified. The c/a ratio revealed the instability of the tetragonal cell and, therefore, its tendency to transform, with a consequent toughness increase.

It was also observed that the amount of stabilizer influenced the c/a ratio; in particular, the lower the stabilizer content, the higher the tetragonality and, therefore, the fracture toughness.

The relationships between microstructure and mechanical properties were investigated. Despite this effect not being completely clear in some cases, it was generally proven that as the average grain size grew, the fracture toughness increased until it approached the critical grain size. On the other hand, flexural strength was not significantly affected by the grain size refinement, probably because of the presence of larger critical defects when TSS was applied instead of SSS.

These experimental results could constitute a scientific base to design new high-performance ZTA composites that applicable in orthopedic and dental implants with high hydrothermal resistance.

Furthermore, an innovative forming technique based on additive manufacturing technology—DLP technique—was successfully tested to produce dental components with zirconia–alumina composites. This technique represents a very interesting perspective for the development of highly customized devices with lower waste and reduced cost that is suitable for small batch production in the biomedical field.

Author Contributions: Conceptualization, G.M.; methodology, G.M.; investigation, G.M., P.F., E.L., F.M., and E.S.; all authors analyzed the data and wrote the paper. All authors have read and agreed to the published version of the manuscript.

Funding: This research received no external funding.

Data Availability Statement: All relevant data are represented in this publication. All raw data and evaluated data are available from the authors upon request.

Conflicts of Interest: The authors declare no conflict of interest.

References

1. Claussen, N. Fracture Toughness of Al_2O_3 with an unstabilized ZrO_2 dispersed phase. *J. Am. Ceram. Soc.* **1976**, *59*, 49–51. [CrossRef]
2. Wang, J.; Stevens, R. Zirconia-toughened alumina (ZTA) ceramics. *J. Mater. Sci.* **1989**, *24*, 3421–3440. [CrossRef]
3. Maji, A.; Choubey, G. Microstructure and mechanical properties of alumina toughened zirconia (ATZ). *Mater. Today Proc.* **2018**, *5*, 7457–7465. [CrossRef]
4. Wimmer, M.A.; Pacione, C.; Yuh, C.; Chan, Y.-M.; Kunze, J.; Laurent, M.P.; Chubinskaya, S. Articulation of an alumina-zirconia composite ceramic against living cartilage—An in vitro wear test. *J. Mech. Behav. Biomed. Mater.* **2020**, *103*, 103531. [CrossRef]
5. Solarino, G.; Piconi, C.; De Santis, V.; Piazzolla, A.; Moretti, B. Ceramic Total knee arthroplasty: Ready to go? *Joints* **2017**, *05*, 224–228. [CrossRef]
6. Piconi, C.; Sprio, S. Zirconia implants: Is there a future? *Curr. Oral Health Rep.* **2018**, *5*, 186–193. [CrossRef]
7. Tsukuma, K.; Ueda, K.; Shimada, M. Strength and fracture toughness of isostatically hot-pressed composites of Al_2O_3 and Y_2O_3-partially-stabilized ZrO_2. *J. Am. Ceram. Soc.* **1985**, *68*, C4–C5. [CrossRef]
8. Tuan, W.H.; Chen, R.Z.; Wang, T.C.; Cheng, C.H.; Kuo, P.S. Mechanical properties of Al_2O_3/ZrO_2 composites. *J. Eur. Ceram. Soc.* **2002**, *22*, 2827–2833. [CrossRef]
9. Shin, Y.-S.; Rhee, Y.-W.; Kang, S.-J.L. Experimental evaluation of toughening mechanisms in alumina-zirconia composites. *J. Am. Ceram. Soc.* **1999**, *82*, 1229–1232. [CrossRef]
10. Hannink, R.H.J.; Kelly, P.M.; Muddle, B.C. Transformation toughening in zirconia-containing ceramics. *J. Am. Ceram. Soc.* **2000**, *83*, 461–487. [CrossRef]
11. Tsukuma, K.; Takahata, T.; Shiomi, M. Strength and fracture toughness of Y-TZP, Ce-TZP, Y-TZP/Al_2O_3, and Ce-TZP/Al_2O_3. In *Advances in Ceramics: Science and Technology of Zirconia III*; Sōmiya, S., Yamamoto, N., Yanagida, H., Eds.; The American Ceramic Society: Columbus, OH, USA, 1988; Volume 24B, pp. 721–728, ISBN 9780916094874.
12. Lange, F.F. Transformation toughening: Part 1 Size effects associated with the thermodynamics of constrained transformations. *J. Mater. Sci.* **1982**, *17*, 225–234. [CrossRef]

13. Garvie, R.C. The occurrence of metastable tetragonal zirconia as a crystallite size effect. *J. Phys. Chem.* **1965**, *69*, 1238–1243. [CrossRef]
14. Gutknecht, D.; Chevalier, J.; Garnier, V.; Fantozzi, G. Key role of processing to avoid low temperature ageing in alumina zirconia composites for orthopaedic application. *J. Eur. Ceram. Soc.* **2007**, *27*, 1547–1552. [CrossRef]
15. Zadorozhnaya, O.Y.; Khabas, T.A.; Tiunova, O.V.; Malykhin, S.E. Effect of grain size and amount of zirconia on the physical and mechanical properties and the wear resistance of zirconia-toughened alumina. *Ceram. Int.* **2020**, *46*, 9263–9270. [CrossRef]
16. Cotič, J.; Jevnikar, P.; Kocjan, A.; Kosmač, T. Complexity of the relationships between the sintering-temperature-dependent grain size, airborne-particle abrasion, ageing and strength of 3Y-TZP ceramics. *Dent. Mater.* **2016**, *32*, 510–518. [CrossRef]
17. Chevalier, J.; Gremillard, L.; Virkar, A.V.; Clarke, D.R. The tetragonal-monoclinic transformation in zirconia: Lessons learned and future trends. *J. Am. Ceram. Soc.* **2009**, *92*, 1901–1920. [CrossRef]
18. Schneider, J.; Begand, S.; Kriegel, R.; Kaps, C.; Glien, W.; Oberbach, T. Low-temperature aging behavior of alumina-toughened zirconia. *J. Am. Ceram. Soc.* **2008**, *91*, 3613–3618. [CrossRef]
19. Chevalier, J.; Grandjean, S.; Kuntz, M.; Pezzotti, G. On the kinetics and impact of tetragonal to monoclinic transformation in an alumina/zirconia composite for arthroplasty applications. *Biomaterials* **2009**, *30*, 5279–5282. [CrossRef]
20. Deville, S.; Chevalier, J.; Fantozzi, G.; Bartolomé, J.F.; Requena, J.; Moya, J.S.; Torrecillas, R.; Díaz, L.A. Low-temperature ageing of zirconia-toughened alumina ceramics and its implication in biomedical implants. *J. Eur. Ceram. Soc.* **2003**, *23*, 2975–2982. [CrossRef]
21. Fabbri, P.; Piconi, C.; Burresi, E.; Magnani, G.; Mazzanti, F.; Mingazzini, C. Lifetime estimation of a zirconia-alumina composite for biomedical applications. *Dent. Mater.* **2014**, *30*, 138–142. [CrossRef]
22. Lughi, V.; Sergo, V. Low temperature degradation -aging- of zirconia: A critical review of the relevant aspects in dentistry. *Dent. Mater.* **2010**, *26*, 807–820. [CrossRef] [PubMed]
23. Deville, S.; Chevalier, J.; Dauvergne, C.; Fantozzi, G.; Bartolomé, J.F.; Moya, J.S.; Torrecillas, R. Microstructural investigation of the aging behavior of (3Y-TZP)–Al_2O_3 composites. *J. Am. Ceram. Soc.* **2005**, *88*, 1273–1280. [CrossRef]
24. Tsubakino, H.; Nozato, R.; Hamamoto, M. Effect of alumina addition on the tetragonal-to-monoclinic phase transformation in zirconia–3 mol% yttria. *J. Am. Ceram. Soc.* **1991**, *74*, 440–443. [CrossRef]
25. Tolkachev, O.S.; Dvilis, E.S.; Alishin, T.R.; Khasanov, O.L.; Miheev, D.A.; Chzhan, T. Assessment of the hydrothermal resistance of Y-TZP ceramics by the degree of tetragonality of major phases. *Lett. Mater.* **2020**, *10*, 416–421. [CrossRef]
26. Zhang, F.; Vanmeensel, K.; Inokoshi, M.; Batuk, M.; Hadermann, J.; Van Meerbeek, B.; Naert, I.; Vleugels, J. Critical influence of alumina content on the low temperature degradation of 2–3 mol% yttria-stabilized TZP for dental restorations. *J. Eur. Ceram. Soc.* **2015**, *35*, 741–750. [CrossRef]
27. Kohorst, P.; Borchers, L.; Strempel, J.; Stiesch, M.; Hassel, T.; Bach, F.W.; Hübsch, C. Low-temperature degradation of different zirconia ceramics for dental applications. *Acta Biomater.* **2012**, *8*, 1213–1220. [CrossRef]
28. Nogiwa-Valdez, A.A.; Rainforth, W.M.; Zeng, P.; Ross, I.M. Deceleration of hydrothermal degradation of 3Y-TZP by alumina and lanthana co-doping. *Acta Biomater.* **2013**, *9*, 6226–6235. [CrossRef]
29. Zhang, F.; Vanmeensel, K.; Inokoshi, M.; Batuk, M.; Hadermann, J.; Van Meerbeek, B.; Naert, I.; Vleugels, J. 3Y-TZP ceramics with improved hydrothermal degradation resistance and fracture toughness. *J. Eur. Ceram. Soc.* **2014**, *34*, 2453–2463. [CrossRef]
30. Gremillard, L.; Chevalier, J.; Epicier, T.; Deville, S.; Fantozzi, G. Modeling the aging kinetics of zirconia ceramics. *J. Eur. Ceram. Soc.* **2004**, *24*, 3483–3489. [CrossRef]
31. Hallmann, L.; Mehl, A.; Ulmer, P.; Reusser, E.; Stadler, J.; Ha, C.H.F.; Zenobi, R.; Stawarczyk, B.; Mutlu, O. The influence of grain size on low-temperature degradation of dental zirconia. *J. Biomed. Mater. Res. B Appl. Biomater.* **2012**, *100*, 447–456. [CrossRef]
32. Lange, F.F. Transformation toughening: Part 3 Experimental observations in the ZrO_2-Y_2O_3 system. *J. Mater. Sci.* **1982**, *17*, 240–246. [CrossRef]
33. Becher, P.F.; Swain, M. V Grain-size-dependent transformation behavior in polycrystalline tetragonal zirconia. *J. Am. Ceram. Soc.* **1992**, *75*, 493–502. [CrossRef]
34. Suresh, A.; Mayo, M.J.; Porter, W.D.; Rawn, C.J. Crystallite and grain-size-dependent phase transformations in yttria-doped zirconia. *J. Am. Ceram. Soc.* **2003**, *86*, 360–362. [CrossRef]
35. Bravo-Leon, A.; Morikawa, Y.; Kawahara, M. Fracture toughness of nanocrystalline tetragonal zirconia with low yttria content. *Acta Mater.* **2002**, *50*, 4555–4562. [CrossRef]
36. Eichler, J.; Rödel, J.; Eisele, U.; Hoffman, M. Effect of Grain size on mechanical properties of submicrometer 3Y-TZP: Fracture strength and hydrothermal degradation. *J. Am. Ceram. Soc.* **2007**, *90*, 2830–2836. [CrossRef]
37. SmarTech Markets Publishing. *Ceramics Additive Manufacturing Markets 2017–2028. An Opportunity Analysis and Ten-Year Market Forecast*; SmarTech Analysis: Crozet, VA, USA, 2018. Available online: https://www.smartechanalysis.com (accessed on 10 September 2020).
38. SmarTech Analysis. *Ceramics Additive Manufacturing Production Markets: 2019–2030*; SmarTech Analysis: Crozet, VA, USA, 2020. Available online: http://www.smartechanalysis.com (accessed on 10 September 2020).
39. Sun, Y.; Wang, C.; Zhao, Z. ZTA Ceramic materials for DLP 3D printing. *IOP Conf. Ser. Mater. Sci. Eng.* **2019**, *678*, 012020. [CrossRef]

40. Wu, H.; Liu, W.; Lin, L.; Li, L.; Li, Y.; Tian, Z.; Zhao, Z.; Ji, X.; Xie, Z.; Wu, S. Preparation of alumina-toughened zirconia via 3D printing and liquid precursor infiltration: Manipulation of the microstructure, the mechanical properties and the low temperature aging behavior. *J. Mater. Sci.* **2019**, *54*, 7447–7459. [CrossRef]
41. Coppola, B.; Lacondemine, T.; Tardivat, C.; Montanaro, L.; Palmero, P. Designing alumina-zirconia composites by DLP-based stereolithography: Microstructural tailoring and mechanical performances. *Ceram. Int.* **2021**, *47*, 13457–13468. [CrossRef]
42. Zhang, X.; Wu, X.; Shi, J. Additive manufacturing of zirconia ceramics: A state-of-the-art review. *J. Mater. Res. Technol.* **2020**, *9*, 9029–9048. [CrossRef]
43. Li, X.; Zhong, H.; Zhang, J.; Duan, Y.; Bai, H.; Li, J.; Jiang, D. Dispersion and properties of zirconia suspensions for stereolithography. *Int. J. Appl. Ceram. Technol.* **2020**, *17*, 239–247. [CrossRef]
44. de Camargo, I.L.; Morais, M.M.; Fortulan, C.A.; Branciforti, M.C. A review on the rheological behavior and formulations of ceramic suspensions for vat photopolymerization. *Ceram. Int.* **2021**, *47*, 11906–11921. [CrossRef]
45. Niihara, K. A fracture mechanics analysis of indentation-induced Palmqvist crack in ceramics. *J. Mater. Sci. Lett.* **1983**, *2*, 221–223. [CrossRef]
46. Li, P.; Chen, I.-W.; Penner-Hahn, J.E. Effect of dopants on zirconia stabilization–An X-ray absorption study: II, tetravalent dopants. *J. Am. Ceram. Soc.* **1994**, *77*, 1281–1288. [CrossRef]
47. Nisticò, R. Zirconium oxide and the crystallinity hallows. *J. Aust. Ceram. Soc.* **2021**, *57*, 225–236. [CrossRef]
48. Jang, J.W.; Kim, D.J.; Lee, D.Y. Size effect of trivalent oxides on low temperature phase stability of 2Y-TZP. *J. Mater. Sci.* **2001**, *36*, 5391–5395. [CrossRef]
49. Zhang, F.; Batuk, M.; Hadermann, J.; Manfredi, G.; Mariën, A.; Vanmeensel, K.; Inokoshi, M.; Van Meerbeek, B.; Naert, I.; Vleugels, J. Effect of cation dopant radius on the hydrothermal stability of tetragonal zirconia: Grain boundary segregation and oxygen vacancy annihilation. *Acta Mater.* **2016**, *106*, 48–58. [CrossRef]
50. Tien, T.Y. Toughened Ceramics. U.S. Patent U.S. 4,886,768A, 12 December 1987.
51. Yoshimura, M. Phase stability of zirconia. *Am. Ceram. Soc. Bull.* **1988**, *67*, 1950–1955.
52. Matsui, K.; Horikoshi, H.; Ohmichi, N.; Ohgai, M.; Yoshida, H.; Ikuhara, Y. Cubic-formation and grain-growth mechanisms in tetragonal zirconia polycrystal. *J. Am. Ceram. Soc.* **2003**, *86*, 1401–1408. [CrossRef]
53. Shimozono, T.; Ikeda, J.; Pezzotti, G. Evaluation of transformation zone around propagating cracks in zirconia biomaterials using raman microprobe spectroscopy. In Proceedings of the Bioceramics 18, Kyoto, Japan, 8–12 December 2005; Nakamura, T., Yamashita, K., Neo, M., Eds.; Trans Tech Publications Ltd.: Bäch, Switzerland, 2006; Volume 309–311, pp. 1207–1210. [CrossRef]
54. Matsumoto, R.L.K. Aging Behavior of Ceria-Stabilized Tetragonal Zirconia Polycrystals. *J. Am. Ceram. Soc.* **1988**, *71*, C128–C129. [CrossRef]
55. Chevalier, J.; Gremillard, L. Ceramics for medical applications: A picture for the next 20 years. *J. Eur. Ceram. Soc.* **2009**, *29*, 1245–1255. [CrossRef]
56. Kim, D.-J. Effect of Ta_2O_5, Nb_2O_5, and HfO_2 alloying on the transformability of Y_2O_3-stabilized tetragonal ZrO_2. *J. Am. Ceram. Soc.* **1990**, *73*, 115–120. [CrossRef]
57. Kim, D.-J.; Tien, T.-Y. Phase Stability and Physical Properties of Cubic and Tetragonal ZrO_2 in the System ZrO_2-Y_2O_3-Ta_2O_5. *J. Am. Ceram. Soc.* **1991**, *74*, 3061–3065. [CrossRef]
58. Ramesh, S.; Gill, C.; Lawson, S. Effect of copper oxide on sintering, microstructure, mechanical properties and hydrothermal ageing of coated 2.5Y-TZP ceramics. *J. Mater. Sci.* **1999**, *34*, 5457–5467. [CrossRef]
59. Magnani, G.; Brillante, A. Effect of the composition and sintering process on mechanical properties and residual stresses in zirconia-alumina composites. *J. Eur. Ceram. Soc.* **2005**, *25*, 3383–3392. [CrossRef]
60. Yoshimura, M.; Yashima, M.; Noma, T.; Sōmiya, S. Formation of diffusionlessly transformed tetragonal phases by rapid quenching of melts in ZrO_2-$RO_{1.5}$ systems (R = rare earths). *J. Mater. Sci.* **1990**, *25*, 2011–2016. [CrossRef]
61. Rice, R.W. Ceramic tensile strength-grain size relations: Grain sizes, slopes, and branch intersections. *J. Mater. Sci.* **1997**, *32*, 1673–1692. [CrossRef]
62. Trunec, M. Effect of grain size on mechanical properties of 3Y-TZP ceramics. *Ceram. Silikaty* **2008**, *52*, 165–171.
63. Casellas, D.; Alcalá, J.; Llanes, L.; Anglada, M. Fracture variability and R-curve behavior in yttria-stabilized zirconia ceramics. *J. Mater. Sci.* **2001**, *36*, 3011–3025. [CrossRef]
64. Chevalier, J.; Liens, A.; Reveron, H.; Zhang, F.; Reynaud, P.; Douillard, T.; Preiss, L.; Sergo, V.; Lughi, V.; Swain, M.; et al. Forty years after the promise of «ceramic steel?»: Zirconia-based composites with a metal-like mechanical behavior. *J. Am. Ceram. Soc.* **2020**, *103*, 1482–1513. [CrossRef]
65. Sadowski, T.; Łosiewicz, K.; Boniecki, M.; Szutkowska, M. Assessment of mechanical properties by nano- and microindentation of alumina/zirconia composites. *Mater. Today Proc.* **2021**, *45*, 4196–4201. [CrossRef]
66. Krell, A. Load dependence of hardness in sintered submicrometer Al_2O_3 and ZrO_2. *J. Am. Ceram. Soc.* **1995**, *78*, 1417–1419. [CrossRef]
67. Chintapalli, R.; Mestra, A.; García Marro, F.; Yan, H.; Reece, M.; Anglada, M. Stability of nanocrystalline spark plasma sintered 3Y-TZP. *Materials* **2010**, *3*, 800–814. [CrossRef]
68. Yao, W.; Liu, J.; Holland, T.B.; Huang, L.; Xiong, Y.; Schoenung, J.M.; Mukherjee, A.K. Grain size dependence of fracture toughness for fine grained alumina. *Scr. Mater.* **2011**, *65*, 143–146. [CrossRef]

69. Borrell, A.; Salvador, M.D.; Peñaranda-Foix, F.L.; Cátala-Civera, J.M. Microwave sintering of zirconia materials: Mechanical and microstructural properties. *Int. J. Appl. Ceram. Technol.* **2013**, *10*, 313–320. [CrossRef]
70. Chen, I.-W.; Wang, X.-H. Sintering dense nanocrystalline ceramics without final-stage grain growth. *Nature* **2000**, *404*, 168–171. [CrossRef]
71. Loong, T.H.; Soosai, A.; Muniandy, S. Effect of temperature and holding time on zirconia toughened alumina (ZTA) prepared by two-stage sintering. *Mater. Sci. Forum* **2021**, *1030*, 11–18. [CrossRef]
72. Sivanesan, S.; Loong, T.H.; Namasivayam, S.; Fouladi, M.H. Two-stage sintering of alumina-Y-TZP (Al_2O_3/Y-TZP) composites. *Key Eng. Mater.* **2019**, *814*, 12–18. [CrossRef]
73. Xiong, Y.; Hu, J.; Shen, Z. Dynamic pore coalescence in nanoceramic consolidated by two-step sintering procedure. *J. Eur. Ceram. Soc.* **2013**, *33*, 2087–2092. [CrossRef]
74. Bergstrom, L. Colloidal Processing of Ceramics. In *Handbook of Applied Surface and Colloid Chemistry*; Holmberg, K., Ed.; John Wiley & Sons, Ltd.: Chichester, UK, 2001; Volume 1, pp. 201–218.